# Inward particle transport by plasma collective modes

# INWARD PARTICLE TRANSPORT BY PLASMA COLLECTIVE MODES

T. ANTONSEN, B. COPPI, R. ENGLADE
Massachusetts Institute of Technology,
Cambridge, Massachusetts,
United States of America

ABSTRACT. A model for the rate of density rise observed when neutral gas is fed into a plasma-containing chamber is presented for regimes where known collisional transport processes do not provide an adequate explanation. A dense layer of cold plasma produced at the edge of the plasma column and the resulting relatively sharp ion temperature gradient, as compared with the local density gradient, can lead to the excitation of electron temperature fluctuations driven by ion drift modes. The net inflow of electrons and ions that is produced by these modes has been included in a one-dimensional transport code used to simulate experiments performed by the Alcator device. The linear and quasi-linear theories of these modes are given for the regimes of interest. The cold-plasma-layer model is also consistent with the presence of an outflow of impurity ions, due to impurity driven modes, that balance the inflow produced by discrete collisions.

## 1. INTRODUCTION

The possibility of controlling the particle density in a magnetically confined plasma permits the realization of regimes with different degrees of collisionality, and, therefore, with different types of transport properties. In addition, by varying the density as a function of time during the plasma heating phase, an optimal sequence of heating processes can be produced [1]. The problem of re-fuelling a thermonuclear reactor is, in fact, related to that of plasma density control.

It has been found experimentally, first in the ST experiment at Princeton [2], then to a remarkable degree in the Alcator experiment [3] at MIT, and by now in a number of other experiments on magnetically confined plasmas, that the peak plasma density can be raised simply by bleeding neutral gas into the plasma chamber during a stable discharge. The only apparent limitation is that the injection of neutral gas should not be so rapid as to induce a disruption of the plasma column by a sequence of processes [1, 4] of the type discussed at the end of this section.

We recall also that when the plasma density is increased in a sequence of experiments, the energy replacement time is observed to improve, while the degree of decontamination from impurity ions coming from the metallic surfaces surrounding the plasma column is also improved. Therefore, hydrogen or deuterium plasmas with good confinement times and an effective charge number of about one can be produced [3].

A transport code [5] developed to simulate the plasma density and temperature profiles obtained in Alcator succeeds well in its task thanks to the adoption of appropriate anomalous transport coefficients as long as the assumed initial density is peaked at the centre and no attempt is made to raise it by providing an influx of neutrals at the wall. In fact, when such an influx is added in order to simulate the bleeding of gas into the plasma chamber and only a collisional description for the inward transport of neutrals is retained, the density profile develops a sharp peak at the outer edge of the plasma column, and, contrary to the experimental observations, only a slow increase of the central density is obtained. Notice that this code [5] contains also the contribution of the inward (Ware) drift of trapped particles which, in the high-density regimes of interest, is not found to be appreciable.

Therefore, we have been led to develop an anomalous transport model based on the excitation of collective modes that can carry plasma from the edge of the plasma column toward its centre. In particular, we assume that in the presence of a vigorous heating power input, such as Ohmic heating as in the case of Alcator, a dense layer of cold plasma is set up at the edge of the column itself. This layer can produce a temperature profile for which the relative temperature gradient $|d \ln T/dr|$ is larger than the relative density gradient $|d \ln n/dr|$. Then ion drift modes which tend to mix the hot- and cold-ion populations can be excited [6, 7]. At the same time, the resulting electron temperature fluctuations associated with the effects of

finite longitudinal electron thermal conductivity, or Landau resonance, can produce a net inward transport of ions and electrons. The rate of this transport is consistent with the needed rise-time of the central density.

As stated, the model assumes that drift waves driven by the ion temperature gradient are excited. The physical mechanism for the instability [6, 7] can be understood by considering the fluid equations for ions in the limit in which the ion motion along the field line is not negligible. In the absence of gradients in density and temperature, a disturbance which causes the ions to move along the field compresses the plasma. This induces a perturbation in the ion pressure and an ambipolar electric field required to maintain quasi-neutrality. The effect of the electric field and the ion pressure perturbation is to resist compression, and the resulting oscillation is an ion acoustic wave.

If a large ion temperature gradient is imposed across the magnetic field, the perturbed ion pressure changes owing to $\vec{E} \times \vec{B}$ motion. That is, the convection of cold ions across the field induces an additional perturbation to the ion pressure. With the proper choice of wave vector $\vec{k}$, a frequency of oscillation exists for which the convective perturbation of the ion pressure is such that the resulting force on the ions enforces compression rather than resisting it. Thus, the perturbation grows.

The threshold for instability is generally given by the condition that the convective perturbation of the ion pressure should overcome the compressional perturbation and the ambipolar electric field. This threshold cannot be calculated directly because it involves the unknown wave frequency, and, therefore, must be determined from the dispersion relation. We recall that, in the case of the more familiar electron drift wave, the electron dissipation drives particles down the density gradient and gives rise to instability. In fact, for this reason the electron drift wave cannot be responsible for inward transport. Here the instability is governed by the ion dynamics, and the electron response can be taken to be adiabatic when the growth of the mode is considered.

Experiments carried out on the Alcator device indicate that a disruptive instability is excited when a rapid density rise is imposed on the plasma column. In fact, the disruption follows a rapid amplification of $m^o = 2$ oscillations. In turn these oscillations are the result of a resistive instability whose growth rate depends critically on the typical plasma parameters at the surface $r = r_2$ where $\iota(r) = 1.2$, $\iota$ being the rotational transform. By programming an appropriate rate of rise of the current we argue that a current skin layer tends to form and local heating around the surface where $\iota(r) = 1/2$ is produced. Then the stability properties of the $m^o = 2$ mode are considerable improved [1] so that it can develop into an oscillation of moderate and steady amplitude. On the other hand, when the cold-plasma layer is allowed to increase excessively the plasma collisionality at the surface $r \cong r_2$, the relevant resistive mode can develop in a regime where its growth rate becomes comparable to or larger than its frequency of oscillation and becomes difficult to saturate. Then a disruption of the plasma column can be produced. The consequence of this is that, to increase the plasma density without inducing a disruption, a simultaneous rise of the plasma current at a sufficiently high rate has to be programmed [1]. In fact, this tends to enhance the current density, by skin effect, around the surface $r \cong r_2$. Thus, the local electron temperature is also increased and the $m^o = 2$ mode is prevented from developing into a macroscopic instability.

The organization of this paper is as follows. In Section 2, we present a linear fluid theory of the ion mixing mode which we find to be valid when $\omega < \nu_i$, where $\omega$ is the mode frequency and $\nu_i$ is the ion collision frequency. In this limit, it is found that transverse ion viscosity and thermal conductivity are important stabilizing effects. In Section 3, we consider the opposite limit of collisionality, $\omega > \nu_i$, where a kinetic treatment of the ions is necessary. Stability criteria are obtained from the resulting dispersion relation with the aid of Nyquist's theorem. Also, the dispersion relation is solved numerically in two interesting limits.

In Section 4, we present a quasi-linear theory of the transport resulting from ion-mixing mode fluctuations. In this section, particle flux and the electron and ion energy fluxes are derived in terms of the unknown spectrum of fluctuations. Separate derivations are given for both collisional and collisionless regimes.

In Section 5, specific estimates of the transport coefficients are made. The result is a set of expressions for the particle and energy fluxes that can be incorporated into a one-dimensional transport code.

In Section 6, we describe a one-dimensional radial transport code designed to model the build-up of density in a magnetically confined plasma column during the injection of neutral gas.

In Section 7, we present numerical simulations obtained with the computer code that model the gas injection experiments in the Alcator tokamak.

Finally, in Section 8, we discuss the relation between the ion-mixing mode transport and the anomalous impurity transport predicted in Ref. [8].

## 2. FLUID THEORY

The ion-mixing mode can be described most easily by a simple analysis based on fluid equations [4, 7, 8]. To illustrate this point, we adopt a guiding-centre description for both electrons and ions, where we neglect, at first, finite-ion-gyroradius effects and refer to a one-dimensional (x-dependent), plane equilibrium configuration (ignoring toroidal and shear effects) in which the magnetic field is in the z-direction. We consider electrostatic modes represented by $\vec{E}_1 = -\nabla\tilde{\phi}$, with $\tilde{\phi} = \tilde{\phi}(x)\exp(ik_y y + ik_z z - i\omega t)$. The relevant wavelengths are larger than the Debye length, and the quasi-neutrality condition $\tilde{n}_i = \tilde{n}_e$ is to be satisfied.

The ions are governed by the equations of continuity, parallel momentum balance, and adiabatic compression:

$$-i\omega\tilde{n}_i + \tilde{v}_{Ex}\frac{\partial n_o}{\partial x} + ik_z n_o \tilde{u}_i = 0 \qquad (2\text{-}1)$$

$$-i\omega m_i n_o \tilde{u}_i = -ik_z(n_o e\tilde{\phi} + \tilde{p}_i) \qquad (2\text{-}2)$$

$$\frac{3}{2}\left(-i\omega\tilde{p}_i + \tilde{v}_{Ex}\frac{\partial p_o}{\partial x}\right) + \frac{5}{2}ik_z p_o \tilde{u}_i = 0 \qquad (2\text{-}3)$$

where $\tilde{v}_{Ex} = -cB^{-1}ik_y\tilde{\phi}$ is the $\vec{E}\times\vec{B}$ drift, $\tilde{p}_i$, $\tilde{n}_i$, and $\tilde{u}_i$ are the perturbed ion pressure, density, and velocity along the magnetic field, and $n_0$ and $p_0$ are the equilibrium ion density and pressure.

We take the response of the electrons to be adiabatic,

$$\tilde{n}_e = n_o\frac{e\tilde{\phi}}{T_e} \qquad (2\text{-}4)$$

Corrections to expression (2-4) that result from dissipative effects will be considered in Section 5. Combining Eqs (2-1) – (2-4) yields the following dispersion relation

$$\frac{3}{2}\omega\left[\frac{m_i}{k_\parallel^2 T_i}\omega(\omega+\omega_*) - \frac{T_e}{T_i}\right] + \frac{3}{2}\omega_*\left(\eta_i - \frac{2}{3}\right) - \frac{5}{2}\omega = 0 \qquad (2\text{-}5)$$

where $\omega_* = cT_e k_y/(eBr_n)$ and $n_0 r_n^{-1} = \partial n_0/\partial x$. Equation (2-5) is a third-order polynomial in $\omega$. The stability criterion on $\eta_i$ is found to be,

$$\eta_i > \frac{2}{3} - \frac{1}{9}C\{1-2[1+A][(1+A^{-1})^{1/2} - 1]\} \qquad (2\text{-}6)$$

where $C = 5/3 + T_e/T_i$ and $A = \omega_*^2 m_i/(k_z^2 T_i 3C)$. The mode frequency satisfies $\omega \sim k_z v_i$, where $\frac{1}{2}m_{i,e}v_{i,e}^2 = T_{i,e}$.

A plot of $\eta_c$, where $\eta_c$ is the critical value of $\eta_i$ required for instability, is shown in Fig.1 as a function of $\omega_*/(k_z v_i)$. As can be seen from Fig.1, if $k_z v_i \ll \omega_*$, the instability criterion becomes simply $\eta_i > 2/3$. The limiting value of 2/3 can be understood in the context of the physical mechanism presented in the introduction. If $\omega \sim k_z v_i \ll \omega_*$, the compression of the plasma along the field is determined by the continuity equation, $n_0\nabla_\parallel\tilde{u}_i = -\tilde{v}_{Ex}\cdot\nabla n_0$. Therefore, to obtain a negative ion pressure perturbation upon compression we must have

$$\frac{3}{2}\vec{\tilde{v}}_{Ex}\cdot\nabla p_o + \frac{5}{2}p_o\nabla_\parallel\tilde{u}_i = \left[1 - \frac{3}{2}\eta_i\right]\vec{\tilde{v}}_{Ex}\cdot\nabla n_o < 0$$

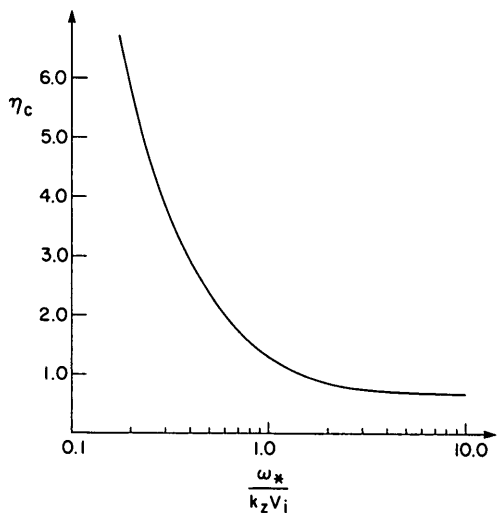


*FIG.1. Stability criterion obtained from Eq. (2–6) with $T_e = T_i$.*

We recall that $\omega_*/(k_z v_i) \cong k_y\rho_i/(k_z r_n)$, for $T_e \sim T_i$ where $\rho_i$ is the ion gyroradius. In order to simulate the effects of toroidal geometry we take $k_z \cong (qR)^{-1}$ which prevents the $\eta_i > 2/3$ limit from being attained for values of $k_y\rho_i$ that are consistent with the use of the given equations. We also recall that the solution of Eq. (2-5) yields $\omega \sim k_z v_i$. Thus, fluid equations will be valid provided $\omega < \nu_{ii}$, where $\nu_{ii}$ is the ion-ion collision frequency. Now we notice that finite-Larmor-radius effects become important for $k_y^2\rho_i^2 \sim 1$. The cross field dissipative effects become important for $\omega \sim \nu_{ii}k_y^2\rho_i^2$. Thus, for the given frequency range, $\omega < \nu_{ii}$, the dissipative effects will dominate.

Accordingly, we re-derive the dispersion relation including in the fluid equations the ion stress tensor and ion thermal conductivity [10]. Here we use particle fluid equations rather than guiding-centre equations. We shall neglect the stress tensor in the perpendicular momentum balance so that the perpendicular ion velocity is given by

$$\vec{v}_\perp = cB^{-1}\vec{b} \times [\nabla \phi + (en)^{-1}\nabla_\perp p]$$

where n and p are the total (perturbed plus unperturbed) ion density and pressure. Thus, $\nabla_\perp \cdot v_\perp = -c(Be)^{-1}(\vec{b}\cdot\nabla_\perp n \times \nabla_\perp p)n^{-2}$ and $\nabla_\perp \cdot nv_\perp = cB^{-1}\vec{b}\cdot\nabla_\perp n \times \nabla_\perp \phi$.

The parallel component of the ion stress can be written

$$(\nabla\cdot\vec{\pi})_z = -\frac{\partial}{\partial z}[\eta_o(\frac{4}{3}\frac{\partial}{\partial z}\tilde{u}_i - \frac{2}{3}\nabla_\perp\cdot\vec{v}_\perp)] - 4\nabla_\perp[\eta_1(\frac{\partial}{\partial z}\vec{v}_\perp + \nabla_\perp\tilde{u}_i)] -2(\vec{b}\times\nabla_\perp)\cdot[\eta_2(\frac{\partial}{\partial z}\vec{v}_\perp + \nabla_\perp\tilde{u}_i)] \quad (2\text{-}7)$$

where $\tilde{u}_i$ is the perturbed ion velocity along the magnetic field, $\eta_0 = 0.96\nu_{ii}^{-1}p_i$ is the compressional viscosity, $\eta_1 = 0.3\nu_{ii}p_i/\Omega_i^2$ is the shear viscosity and $\eta_2 = 0.50\, p_i/\Omega_i$ is the collisionless viscosity. The compressional term can be neglected because it is smaller than the ion inertial term by $k_z v_i/\nu_{ii}$ (here we note that

$$n_o\frac{\partial\tilde{u}_i}{\partial z} \sim \nabla_\perp n\vec{v}_\perp$$

from the continuity equation). Given that $\partial/\partial_z \ll \nabla_\perp$ the remaining terms become,

$$(\nabla\cdot\vec{\pi})_z = +4k_y^2\eta_1\tilde{u}_i - ik_y\Omega_i\tilde{u}_i\frac{\partial p_o}{\partial x}m_i^{-1}$$

Substituting the given form of the stress into the parallel-momentum balance yields,

$$(\omega_o + \frac{6}{5}i\gamma)k_\parallel\tilde{u}_i = \frac{T_i k_\parallel^2}{m_i}(\frac{e\tilde{\phi}}{T_i} + \frac{\tilde{p}}{p_o}) \quad (2\text{-}8)$$

where

$$\omega_o = \omega - k_y(\partial p_o/\partial x)(m_i\Omega_i)^{-1},\quad \gamma = \nu_{ii}k_y^2T_i/(m_i\Omega_i^2)$$

and quantities with a tilde are of first order in the perturbation.

Substitution of the given form of $\vec{v}_\perp$ into the continuity equation and the energy equation yields,

$$(\omega_o + \omega_*)\frac{e\tilde{\phi}}{T_e} = k_z\tilde{u}_i \quad (2\text{-}9)$$

and

$$\frac{3}{2}\omega_o\frac{\tilde{p}}{p_o} + \frac{3}{2}\omega_*(1+\eta_i)\frac{e\tilde{\phi}}{T_e} - \frac{5}{2}k_\parallel\tilde{u}_i = 2i\gamma(\frac{e\tilde{\phi}}{T_e} - \frac{\tilde{p}}{p_o}) \quad (2\text{-}10)$$

where we have eliminated $\tilde{n}/n_0$ by using the adiabatic electron response. The term on the right-hand side of Eq. (2-10) results from the finite thermal conductivity across the field line. The longitudinal thermal conductivity can be neglected owing to the smallness of $k_z v_i/\nu_{ii}$. Equations (2-8), (2-9) and (2-10) can be combined to yield the following dispersion relation:

$$[\frac{3}{2}\omega_o + 2i\gamma][\frac{m_i}{k_\parallel^2T_i}(\omega_o + \frac{6}{5}i\gamma)(\omega_o + \omega_*) - \frac{T_e}{T_i}] + \frac{3}{2}\omega_*(1+\eta_i) - \frac{5}{2}(\omega + \omega_*) - 2i\gamma = 0 \quad (2\text{-}11)$$

which is of third order in $\omega_0$. With the aid of Nyquist's criterion we can obtain necessary and sufficient conditions for instability:

$$\frac{1}{2}(\eta_i - \frac{2}{3}) - \frac{8}{5}\hat{\gamma}^2 \gtrless \frac{1}{2}[\frac{8}{5}\hat{\gamma}^2 + \frac{1}{2}\frac{T_e}{T_i} + \frac{5}{6} - \frac{5}{19}(1 + \frac{T_e}{T_i})] \times [\pm(1+20(1+\tau)/9\zeta_*^2)^{1/2} - 1] \quad (2\text{-}12)$$

where $\hat{\gamma}^2 = \nu_{**}k_y^2T_i/(m\Omega_i^2)$, $\zeta_* = \omega_*/(k_z v_i)$, $\nu_{**} = \nu_{ii}/k_z v_i$, and $\tau = T_e/T_i$.

The stability criteria for positive $\eta_i$ are plotted in Fig.2 as a function of $\hat{\gamma}$ for different values of $(k_z r_n)^2\nu_{**}$. That is, in plotting Eq. (2-12) we have taken into consideration the $k_y\rho_i$ dependence of $\zeta_*^2$ by writing $\zeta_*^2 = 2\hat{\gamma}/[(k_z r_n)^2\nu_{**}]$. As can be seen, viscosity and transverse thermal conductivity have a strong stabilizing effect, and the mode will in general be stabilized at perpendicular wavelengths for which finite-Larmor-radius effects are negligible.

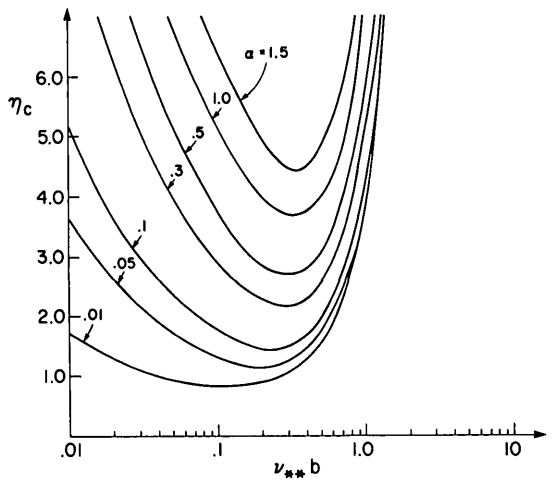


*FIG.2. Stability criteria obtained from Eq. (2–12) when dissipative effects are included. Here,* $\nu_{**} = \nu_{ii}/|k_z v_i|$, $b = T_i k_y^2/(m_i \Omega_i^2)$, $T_e = T_i$, $\alpha = (k_z r_n)^2 \nu_{**}$

## 3. COLLISIONLESS THEORY

In this section we derive the ion response from the Vlasov equation in the collisionless limit. Included in our analysis are finite-Larmor-radius effects. We expect these results to hold when $\omega \sim k_z v_i > \nu_{ii}$.

The perturbed ion distribution function obtained by solving the linearized Vlasov equation by using the method of characteristics is

$$\tilde{f}_i = -\frac{e\tilde{\phi}}{T_i}[f_o + i\omega I f_o - i\omega_{*i} r_n \frac{\partial}{\partial x} I f_o] \quad (3\text{-}1)$$

where

$$f_o = n_o(x)(2\pi T_i(x)/m_i)^{-3/2}\exp(-\tfrac{1}{2} m_i v^2/T_i(x))$$

$$\omega_{*i} = k_y c T_i/(e B r_n), n_o r_n^{-1} = dn_o/dx, \Omega_i = eB/(m_i c)$$

and

$$I = \int_{-\infty}^{o} dt' \exp[\frac{ik_y v_y}{\Omega_i}\sin\Omega_i t' + i\frac{k_y v_x}{\Omega_i}(\cos\Omega_i t' - 1) + ik_z v_z t' - i\omega t'] \quad (3\text{-}2)$$

In deriving Eq. (3-1), we have assumed that the scale length for variation of $n_0(x)$ and $T_i(x)$ is large compared to an ion Larmor radius and we have neglected the x-dependence of $\tilde{\phi}$.

The perturbed ion density can be obtained from Eq. (3-1) by integrating $\tilde{f}$ over all velocities. Using the following expressions,

$$\int d^3\vec{v} f_o = n_o \quad (3\text{-}3)$$

$$\int d^3\vec{v} f_o I = n_o \int_{-\infty}^{o} dt' \exp(-b(1-\cos\Omega_i t') - i\omega t' - k_z^2 v_i^2 t'^2/4)$$

$$\simeq -iI_o(b)\exp(-b)|k_z v_i|^{-1} Z(\omega/|k_z v_i|) n_o \quad (3\text{-}4)$$

where $b = k_y^2 T_i/(m_i\Omega_i^2)$, $I_0(b)$ is the modified Bessel function, $Z(\zeta)$ is the plasma dispersion [11], and we assume $\omega, k_z v_i \ll \Omega_i$ in obtaining Eq. (3-4), we find

$$\frac{\tilde{n}_i}{n_o} = -\frac{e\tilde{\phi}}{T_e}\{\frac{T_e}{T_i}[1 + \exp(-b) I_o(b) \frac{\omega}{|k_z v_i|} Z(\frac{\omega}{k_z v_i})] - \frac{\omega_*}{|k_z v_i|}\exp(-b) I_o(b)[Z(\frac{\omega}{k_z v_i}) + \eta_i(\frac{\omega}{k_z v_i} + (\frac{\omega^2}{k_z^2 v_i^2} - \frac{1}{2} - bG) Z(\frac{\omega}{k_z v_i}))]\} \quad (3\text{-}5)$$

where $\eta_i = d\ln T_i/d\ln n_0$, $G = [1 - I_1(b)/I_0(b)]$, $v_{e,i} = (2T_{e,i}/m_{e,i})^{1/2}$. The electrons are assumed to respond adiabatically to lowest significant order in $\omega/k_z v_e$ (we consider $\omega \sim k_z v_i$),

$$\frac{\tilde{n}_e}{n_o} = \frac{e\tilde{\phi}}{T_e} \quad (3\text{-}6)$$

Modifications to Eq. (3-6) that result from wave-particle resonance in the collisionless case or finite thermal conductivity along the field line in the collisional case will be considered in Section 5. These corrections are small and will not greatly influence the dispersion relation. However, the small corrections provide the phase difference between $\tilde{n}_e$ and $\tilde{\phi}$ necessary to produce inward particle transport.

Using Eqs (3-5) and (3-6) and the quasi-neutrality condition, $\tilde{n}_e/n_0 = \tilde{n}_i/n_0$, we obtain the dispersion relation

$$F(\zeta) \equiv 1 + \tau[1+S_0\zeta Z(\zeta)] - \zeta_* S_0\{Z(\zeta) + \eta_i[\zeta+(\zeta^2 - \tfrac{1}{2})Z(\zeta) - b\,GZ(\zeta)]\} = 0 \qquad (3\text{-}7)$$

where $\zeta = \omega/|k_z v_i|$, $\zeta_* = \omega_*/|k_z v_i|$, $S_0 = \exp(-b)I_0(b)$, $S_1 = \exp(-b)I_1(b)$, and $\tau = T_e/T_i$. The condition for a growing solution ($\mathrm{Im}\,\zeta > 0$) will be determined from Eq. (3-7) with the aid of Nyquist's theorem. In addition, numerical solutions of Eq. (3-7) will be presented. The fluid result [4, 7, 8] can be recovered from Eq. (3-7) in the limit $\zeta, \eta_i \gg 1$, $b \ll 1$,

$$1 - \frac{1}{2}\frac{T_e}{T_i}\frac{k_z^2 v_i^2}{\omega^2} + \frac{\omega_*}{\omega}\left(1 + \eta_i \frac{k_z^2 v_i^2}{2\omega^2}\right) = 0 \qquad (3\text{-}8)$$

which for $\eta_i \gg \omega_*^2/(k_z v_i)^2$ and $\eta_i \omega_*/(k_z v_i) \gg 1$ gives

$$\omega^3 = -\frac{1}{2}\eta_i \omega_* k_z^2 v_i^2 \qquad (3\text{-}9)$$

In the limit $\zeta_* S_0 \gg 1$ and $\eta_i \sim 1$ Eq. (3-7) possesses a purely growing mode [12] which satisfies

$$Z\left(\frac{\omega}{k_z v_i}\right) + \eta_i\left[\frac{\omega}{k_z v_i} + \left(\frac{\omega^2}{k_z^2 v_i^2} - \frac{1}{2} - bG\right) Z\left(\frac{\omega}{k_z v_i}\right)\right] = 0$$

We shall find from the numerical solutions of Eq. (3-7) that the parameter regimes of interest in existing experiments on magnetically confined plasmas are such that neither of the limiting cases just discussed are applicable.

We wish to determine if there are any roots of the equation $F(\zeta) = 0$, where $F(\zeta)$ is defined in Eq. (3-7), for $\zeta$ in the half-plane $\mathrm{Im}\,\zeta > 0$. To do this, we evaluate $F(\zeta)$ along a contour consisting of the real-$\zeta$-axis and a semi-circular arc at $|\zeta| \to \infty$ in the upper half-$\zeta$-plane. The real and imaginary values of $F(\zeta)$ for $\zeta$ on this contour are plotted against each other and define a contour in the F-plane. As the contour in the $\zeta$-plane is followed in the counter-clockwise sense the net counter-clockwise encirclement of the origin in the F-plane will be the number of solutions of Eq.(3-7) for $\mathrm{Im}\,\zeta > 0$.

For $|\zeta| \gg 1$ the asymptotic expression for $F(\zeta)$ is given by

$$F(\zeta) \sim 1 + \tau(1-S_0) + \zeta_* S_0[1-\eta_i bG]\zeta^{-1} \qquad (3\text{-}10)$$

Thus, for large $\zeta$, $F(\zeta)$ tends to the positive constant $1+\tau(1-S_0)$. For $\zeta$ on the real axis the imaginary part of $F(\zeta)$ is given by

$$\mathrm{Im}\{F(\zeta)\} = \pi^{1/2}\exp(-\zeta^2)S_0\{\tau\zeta - \zeta_* \times [1+\eta_i(\zeta^2 - 1/2 - bG)]\} \qquad (3\text{-}11)$$

Thus, for large real $\zeta$,

$$\mathrm{Im}\{F(\zeta)\} \gtrless 0 \quad \text{if} \quad -\zeta_*\eta_i \gtrless 0$$

The contour in the F-plane will cross the real F axis for values of $\zeta$ for which $\mathrm{Im}\{F(\zeta)\} = 0$, that is

$$\tau\zeta - \zeta_*[1+\eta_i(\zeta^2 - 1/2 - bG)] = 0 \qquad (3\text{-}12)$$

If there are no real solutions to Eq. (3-12) then the contour cannot encircle the origin and no instability exists. If two real solutions of Eq. (3-12) exist, they are given by

$$\zeta_{1,2} = \frac{1}{2}\left[\frac{\tau}{\zeta_*\eta_i} \pm \left(\frac{\tau^2}{\zeta_*^2\eta_i^2} - 4\left[\frac{1}{\eta_i} - \left[\frac{1}{2} + bG\right]\right]\right)^{1/2}\right] \qquad (3\text{-}13)$$

where we choose to label $\zeta_1$ and $\zeta_2$ such that $\zeta_1 < \zeta_2$. Using Eqs (3-8) and (3-13), the real part of $F(\zeta_{1,2})$ is found to be

$$R_e(F(\zeta_{1,2})) = 1 + \tau - \zeta_* S_0 \eta_i \zeta_{1,2} \qquad (3\text{-}14)$$

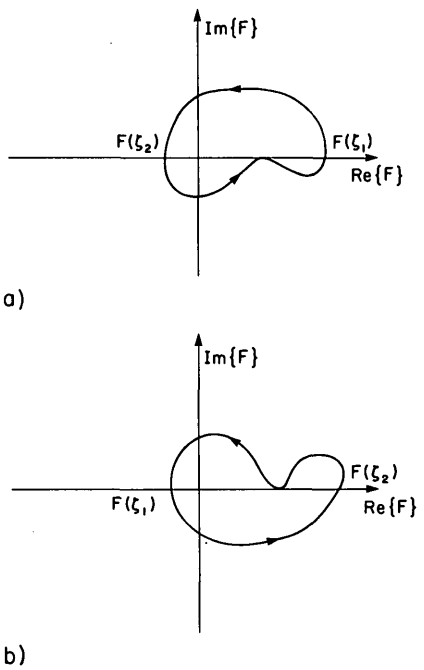


*FIG.3. Nyquist plots of $F(\zeta)$, where $F(\zeta)$ is given by Eq. (3–7), for a) $\zeta_*\eta_i > 0$, b) $\zeta_*\eta_i < 0$, $\zeta \equiv \omega/|k_\parallel v_i|$.*

We first consider $\zeta_* \eta_i > 0$; in this case the contour is of the type shown in Fig.3a. From Eq. (3-14) we see that $F(\zeta_1) > F(\zeta_2)$. Thus, the necessary conditions for instability are $F(\zeta_2) < 0$ and $F(\zeta_1) > 0$.

Secondly, we consider $\zeta_* \eta_i < 0$, in which case the contour is of the type shown in Fig.3b. From Eq. (3-14) we see that $F(\zeta_2) > F(\zeta_1)$ and thus the necessary conditions for instability are $F(\zeta_2) > 0$ and $F(\zeta_1) < 0$. Substituting the known values of $\zeta_{1,2}$ into Eq. (3-14), we find the necessary and sufficient conditions for instability in both cases to be either

$$\eta_i > (1+2b\,G)^{-1}\{1+(1+\frac{\tau^2}{\zeta_*^2}[\frac{1}{2} + bG]\,[(\frac{2}{S_o}(1+\tau^{-1})-1)^2-1]\,)^{1/2}\} \qquad (3\text{-}15a)$$

or

$$\eta_i < (1+2b\,G)^{-1}\{1-(1 + \frac{\tau^2}{\zeta_*^2}\,[\frac{1}{2}+b\,G][(\frac{2}{S_o}(1+\tau^{-1})-1)^2-1]\,)^{1/2}\} \qquad (3\text{-}15b)$$

In all cases, only one unstable mode is possible.

Condition (3-15a) is plotted in Fig.4 as a function of b for various values of $k_z r_n$ and $\tau = 1$. For a given value of $k_z r_n$ the most unstable perpendicular wavelengths occur for $b \sim 1$. If we put $b = 1$, $\tau = 1$, and $k_z \cong (Rq)^{-1}$ in Eq. (3-15a) we obtain

$$\eta_i \gtrless \frac{1}{2}[1 \pm (1+113(r_n/Rq)^2)^{1/2}] \qquad (3\text{-}16)$$

which gives a general stability criterion for a toroidal plasma with major radius R.

Equation (3-7) can be numerically solved in the following way. For fixed values of b and $\tau$ one can pick the real and imaginary parts of $\zeta$, the mode frequency. Then using the tabulated values of the plasma dispersion function [11] Eq. (3-7) yields two algebraic equations for $\zeta_*$ and $\eta_i$ which are readily solved. Repeating the procedure for many values of $\zeta$ yields contour plots in the $\zeta_* - \eta_i$ plane of constant real and imaginary frequency.

Two examples of these plots are shown in Fig.5 for $b \gg 1$, and $b \ll 1$. For the relevant regimes of the parameters $\zeta_* S_0$ and $\eta_i$ ($10 > \zeta_* S_0, \eta_i$) the mode has $\gamma \sim \omega_r \sim k_z v_i$. Therefore, neither of the approximations to Eq. (3-7) discussed previously are appropriate.

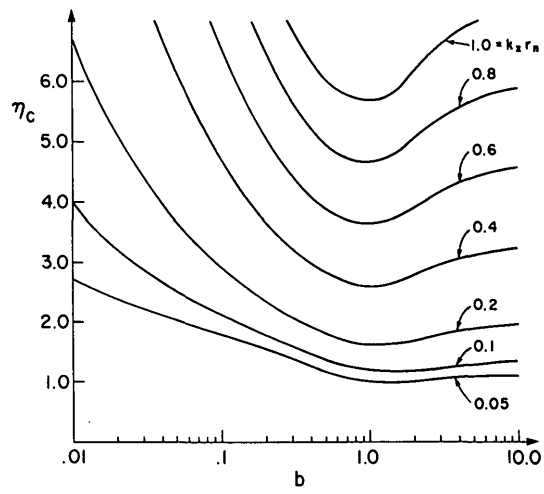


*FIG.4. Collisionless stability criteria for $\eta_i > 0$, where $b = T_i k_y^2/(m_i \Omega_i^2)$.*

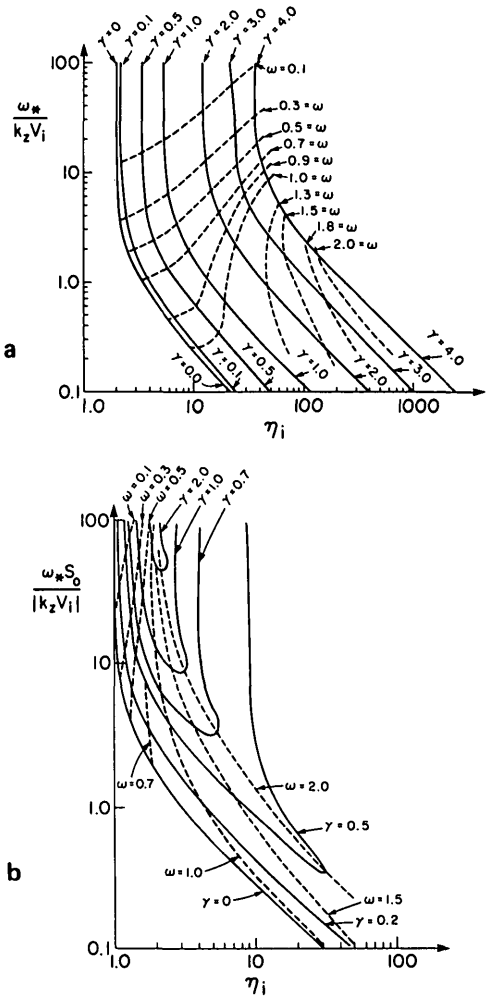


*FIG.5. Contours of constant growth rate and frequency in the collisional regime for a) $b = T_i k_y^2/(m_i \Omega_i^2) < 1$; b) $T_i k_y^2/(m_i \Omega_i^2) > 1$.*

We have presented a linear theory of the stability of electrostatic ion drift modes in the collisional and collisionless regimes neglecting the effects of magnetic shear. The influence of shear on the temperature gradient driven 'quasi-flute mode' in the collisionless slab model was examined in Refs [7, 13] and found to be unimportant. In addition, in toroidal geometry the effect of magnetic shear is modified by the tendency of the modes to become localized in the poloidal angle [14], and the dispersion relation we have derived may be extended approximately to these modes by taking $k_{\|} = (Rq)^{-1}$.

## 4. QUASI-LINEAR TRANSPORT

In this section we shall examine the quasi-linear effect of ion mixing mode fluctuations. In the linear stability theory we found that the electrons respond nearly adiabatically to the fluctuating electrostatic potential, in the sense that $\tilde{n} \cong n_0 e\tilde{\phi}/T_e$. If this relation held exactly, then the density and $\vec{E} \times \vec{B}$ drift velocity perturbations would be such that no particle transport would result. This occurs because the density and velocity are 90° out of phase. Thus, departures from adiabatic response that provide a phase difference between $\tilde{n}_e$ and $\tilde{\phi}$ will give rise to particle transport.

The two mechanisms that we consider to produce the required phase shift are finite electron thermal conductivity along the field in the collisional limit and Landau resonance in the collisionless limit. Once the corrections to the electron density perturbation have been calculated, it must be verified that they are small enough not to alter the dispersion relations derived previously. Our approach in this section will be to calculate the quasi-linear transport for electrons and ions in both the collisional and collisionless regimes and then verify that the linear corrections to the electron response to not greatly influence the stability criteria we gave earlier.

The validity of quasi-linear theory as applied to these modes is questionable owing to the fact that the growth rate and oscillation frequency can be comparable. If such is the case, we expect that our calculations, although numerically inaccurate, give an indication of the direction and magnitude of the various flows. This problem is actually less severe than it may seem because the quasi-linear transport causes the density and ion temperature profiles to evolve toward a more stable state. Thus, the profiles are never forced into a highly unstable state and in many cases the assumption $\gamma < \omega_r$ is satisfied.

We shall assume that collisions are sufficiently strong to maintain the distribution functions near Maxwellian. Examination of the relevant equations indicates that collisions will be strong enough provided $(\nu_{ii} Rq/v_i) > |e\tilde{\phi}/T_i|^2$ which is well satisfied in Alcator.

The expressions for the quasi-linear heat and particle fluxes resulting from electrostatic fluctuations valid in the collisionless limit are given by [15, 16]

$$Q_\sigma = -\int d^3\vec{v} \,\langle i\tilde{\phi}'\,(k'_y \tfrac{1}{2}v^2 + v_y(k'_z v_z + k'_y v_y))\, m_\sigma c \tilde{f}_\sigma B^{-1}\rangle \qquad (4\text{-}1)$$

and

$$\Gamma_\sigma = -\int d^3\vec{v} \,\langle i k'_y \tilde{\phi} c B^{-1} \tilde{f}_\sigma\rangle \qquad (4\text{-}2)$$

$\tilde{f}_\sigma$ is the linear perturbed distribution function for species $\sigma$, $Q_\sigma$ is the energy flux, and $\Gamma_\sigma$ the particle flux. Equations (4-1) and (4-2) apply to ions and electrons if $\omega > \nu_\sigma$. If $\nu_e > |\omega|$, a fluid description of the electrons in which finite thermal conductivity along the field line is accounted for is appropriate.

We first consider Eqs (4-1) and (4-2) as they apply to electrons. Using methods analogous to those of Section 3 we find in the limit $k_\perp \rho_e \ll 1$, $\omega \ll \Omega_e$,

$$\tilde{f}_e = -\frac{e\tilde{\phi}}{T_e}\left[-f_o + \left(1 + \frac{\omega_{*e}}{\omega} r_n \frac{\partial}{\partial x}\right) \frac{\omega}{\omega - k_z v_z} f_o\right] \qquad (4\text{-}3)$$

Substituting Eq. (4-3) into Eq. (4-2) and using the facts, $\omega < \omega_{*e}, \omega/|k_z v_e| \ll 1, Z(\omega/|k_z v_e|) \cong i\pi^{1/2}$, we obtain

$$\Gamma = -\pi^{1/2} \sum \left|\frac{e\phi}{T_e}\right|^2 \frac{c^2 T_e^2}{e^2 B^2} \frac{k_y^2 n_o}{r_n |k_z v_e|} \left[1 - \tfrac{1}{2}\eta_e\right]$$

$$= -D\left[\frac{\partial n_o}{\partial x} - \frac{n_o}{2T_e}\frac{\partial T_e}{\partial x}\right] \qquad (4\text{-}4)$$

and

$$Q_e = -D\left[n_o \frac{\partial T_e}{\partial x} + 2\, T_e \frac{\partial n_o}{\partial x}\right] \qquad (4\text{-}5)$$

where

$$D \equiv \sum_k \pi^{1/2} \left|\frac{e\tilde{\phi}}{T}\right|^2 \frac{c^2 T_e^2}{e^2 B^2} \frac{k_y^2}{|k_z v_e|} \qquad (4\text{-}6)$$

In parameter regimes in which a fluid description of the electrons is valid the particle and energy flux of electrons are given by

$$\Gamma_e = \langle \tilde{v}_{Ex} \tilde{n}_e \rangle \tag{4-7}$$

and

$$Q_e = \frac{3}{2} \langle \tilde{v}_{Ex} (n_o \tilde{T}_e + \tilde{n}_o T_e) \rangle \tag{4-8}$$

The perturbed velocity, density, and temperature appearing in Eqs (4-7) and (4-8) are determined from the linearized equations of continuity, momentum balance along the field line, and heat including thermal conductivity along the field line:

$$\frac{\partial \tilde{n}}{\partial t} + \tilde{v}_{Ex} \frac{\partial n_o}{\partial x} + n_o \frac{\partial \tilde{u}_c}{\partial z} = 0 \tag{4-9}$$

$$\frac{\partial}{\partial z} (-e\tilde{\phi} n_o + \tilde{n}_e T_e + (1+\alpha_t) n_o \tilde{T}_e) = 0 \tag{4-10}$$

$$n_o \frac{3}{2} \left[ \frac{\partial \tilde{T}_e}{\partial t} + \tilde{v}_{Ex} \frac{\partial T_e}{\partial x} \right] + T n_o \frac{\partial \tilde{u}_e}{\partial z} = \frac{\partial}{\partial z} \frac{m_e T_e \chi_e}{m_e \nu_e} \frac{\partial \tilde{T}_e}{\partial z} \tag{4-11}$$

where $\tilde{v}_{Ex} = -ik_y \tilde{\phi}_c / B$, $\alpha_t = 0.71$, and $\chi_e = 3.16$ [10]. In the limit $k_z^2 T_e \chi_e / (m_e \nu_e \omega) \gg 1$ we obtain from Eq. (4-11)

$$\frac{\tilde{n}_e}{n_o} = \left\{ 1+i \left[ 1+\frac{\omega_{*e}}{\omega} (1-\frac{3}{2}\eta_e) \right) \frac{m_e \nu_e \omega (1+\alpha_t)}{k_z^2 T_e \chi_e} \right] \right\} \frac{e\tilde{\phi}}{T_e} \tag{4-12}$$

and

$$\frac{\tilde{n}_e}{n_o} + \frac{\tilde{T}_e}{T_e} (1+\alpha_t) = \frac{e\tilde{\phi}}{T_e} \tag{4-13}$$

which yield

$$\Gamma = -\frac{2}{\pi^{1/2}} \frac{\nu_e (1+\alpha_t)}{\chi_e \nu_e} \ll \left| \frac{1}{k_z} \right| \gg D \left[ \frac{\partial n_o}{\partial x} - \frac{3}{2} \frac{n_o}{T_e} \frac{\partial T_e}{\partial x} \right] \tag{4-14}$$

$$Q_e = \frac{3}{2} \frac{\alpha_t}{1+\alpha_t} \Gamma T_e \tag{4-15}$$

The double angular brackets indicate an average over wave vectors. For example, the average of a quantity A(k) is given by

$$\langle\langle A(k) \rangle\rangle = \sum_k \left| \frac{e\tilde{\phi}}{T_e} \right|^2 \frac{k_y^2}{|k_z v_e|} A(k) \Big/ \sum_k \left| \frac{e\tilde{\phi}}{T_e} \right|^2 \frac{k_y^2}{|k_z v_e|} \tag{4-16}$$

which depends on the spectrum of fluctuations. These averages will be estimated in the next section.

Equations (4-4) and (4-14) are of similar form. Both indicate that the particle flux induced by the ion mixing mode contains two components; one driven by the density gradient and one driven by the electron temperature gradient. The component of the flux driven by the density gradient is directed in such a way so as to carry particles down the density gradient, i.e. normal diffusion. The component of the flux driven by the electron temperature gradient is directed in such a way so as to carry particles up the temperature gradient. Inward transport results (for normal density and temperature profiles) if the component of the flux driven by the temperature gradient exceeds that driven by the density gradient. The condition for this to occur is given by $\eta_e > 2/3$ in the collisional case and $\eta_e > 2$ in the collisionless case. We recall that if the fluctuations were of the electron drift type, rather than the ion mixing mode, net particle transport up the density gradient could not occur because in this case the particular electron drift mode would necessarily be linearly stable.

The determination of the ion energy flux is straightforward but tedious. Substitution of Eq. (2-2) into Eq. (4-1) yields

$$Q_i = \sum_k \frac{m_i c}{B} \tilde{\phi}_k^* i k_y \tilde{H}(k) \tag{4-17}$$

where

$$\tilde{H}(k) = -\frac{e\tilde{\phi}}{T_i} \left[ 1 - \frac{\omega_{*i}}{\omega} r_n \frac{\partial}{\partial x} \right] \frac{n_o v_i^2}{2} \{ \zeta Z(\zeta) [(2-b+\zeta^2) S_o + b S_1] + \zeta^2 S_o \} - \frac{e\tilde{\phi}}{T_i} \frac{5}{4} n_o v_i^2 \tag{4-18}$$

Upon performing the indicated differentiation and saving only the imaginary terms, for $\mathrm{Im}\,\omega = 0$, we obtain

$$\tilde{H}(k) = -\frac{e\tilde{\phi}}{T} \{ S_o \zeta Z_i(\zeta) - \frac{\omega_{*i}}{\omega} S_o \zeta Z_i(\zeta) [1+\eta_i (\zeta^2 - \tfrac{1}{2} - bG)] \frac{n_o v_i^2}{2} \times [2+(\zeta^2 - b + (b-1)\frac{S_1}{S_o})] + \frac{e\tilde{\phi}}{T_i} \frac{\omega_*}{|k_z v_i|} n_o v_i^2 \eta_i K(b) Z_i(\zeta) \tag{4-19}$$

where $2K(b) = 2S_0 - S_1 - 2b(S_0 - S_1) + (b-1)[b(S_0 - S_1)(1 + S_1/S_0) - S_1]$. A plot of K(b) appears in Fig.6. The first term in Eq. (4-19) is proportional to the imaginary part of the perturbed ion density. This yields a convective energy flux. The second term yields a conductive energy flux. Thus, we obtain for the total energy flux:

$$Q_i = 2T_i\Gamma \left\langle\left\langle 1 + \frac{1}{2}(\zeta^2 - b + (b-1)S_1/S_0)\right\rangle\right\rangle - \left(\frac{v_e}{v_i}\right)\frac{1}{\pi^{1/2}} 2D \left\langle\left\langle Z(\zeta)K(b)\right\rangle\right\rangle n_i \frac{\partial T_i}{\partial x} \qquad (4\text{-}20)$$

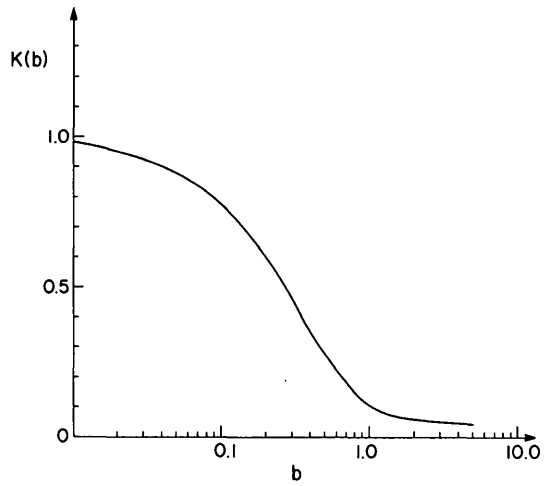


*FIG.6. The function K(b) where K(b) is defined following Eq. (4–19).*

In the collisional limit the ion energy flux must be determined from a fluid treatment of the ions. The ion energy flux is given by

$$Q_i = \frac{3}{2}\langle \tilde{v}_x^* \tilde{p}_i \rangle \qquad (4\text{-}21)$$

$\tilde{p}_i$ is obtained from the parallel momentum balance,

$$k_z \tilde{p}_i = (\omega_o + \frac{5}{6} i\gamma) m n_o \tilde{u}_i - k_z(q\tilde{\phi} n_o - \alpha_t n_o \tilde{T}_e) \qquad (4\text{-}22)$$

and $\tilde{u}_i$ is obtained from the continuity equation

$$k_z \tilde{u}_i = \omega_o \frac{\tilde{n}_i}{n_o} + \omega_* \frac{e\tilde{\phi}}{T_e}$$

Thus, we find

$$Q_i = \frac{3}{2}\tilde{v}_{Ex}(\alpha_t n_o \tilde{T}_e - e\tilde{\phi} + m_i n_o k_z^{-2}(\omega_o + \frac{5}{6} i\gamma)(\omega_o \tilde{n}_i/n_o + \omega_* \frac{e\tilde{\phi}}{T_e})) \qquad (4\text{-}23)$$

The electron temperature perturbation can be eliminated using Eq. (4-10), we use the quasi-neutrality condition to equate $\tilde{n}_e$ and $\tilde{n}_i$, and we find that terms of the form $\langle \tilde{v}_{Ex}^* \tilde{\phi} \rangle$ do not contribute. Thus, $Q_i$ reduces further to

$$Q_i = \frac{3}{2}\langle \tilde{v}_{Ex}^* \tilde{n}_e [\zeta_o^2 2T_i - T_e \alpha_t (1+\alpha_t)^{-1}] \rangle + \frac{5}{2}\langle \tilde{v}_{Ex}^* n_o T_i (\zeta_o \frac{\tilde{n}_e}{n_o} + \zeta_* \frac{e\tilde{\phi}}{T_e})\, i\hat{\gamma} \rangle \qquad (4\text{-}24)$$

where $\zeta_0 = \omega_0/(k_z v_i)$, $\zeta_* = \omega_*/(k_z v_i)$, $\hat{\gamma} = \gamma(k_z v_i)^{-1}$. The first term in Eq. (4-24) is the convective energy flux. In the second term of Eq. (4-24) we recall $\tilde{n}_e/n_0 \cong e\tilde{\phi}/T_e$ and $\omega_0 < \omega_*$. Therefore, we obtain for $Q_i$

$$Q_i = \frac{3}{2}\Gamma \left\langle\left\langle \zeta_o^2 - \frac{T_e}{2T_i}\alpha_t(1+\alpha_t)^{-1}\right\rangle\right\rangle > > -\frac{5}{2} T_i D \left\langle\left\langle \hat{\gamma} \gg \left(\frac{v_e}{v_i \pi^{1/2}}\right)\right\rangle\right\rangle \frac{\partial n}{\partial x} \qquad (4\text{-}25)$$

We now examine the effect of the dissipative corrections to the electron response on the linear dispersion relations. First we consider the collisionless case. The corrections to $\tilde{n}_e/n_0$ are of order $\omega_*/|k_z v_e|$. That is,

$$\frac{\tilde{n}_e}{n_o} = \frac{e\tilde{\phi}}{T_e}\left[1 + \mathcal{O}\left(\frac{\omega_*}{k_z v_e}\right)\right]$$

If this is inserted in Eq. (2-8) we see that the ion terms which are of order $\omega_*/|k_z v_i|$ will dominate.

In the collisional case the correction to the electron response is of order $\omega_* \nu_e/(k_z^2 v_e^2)$. The ion terms are again of order $\omega_*/|k_z v_i|$. Thus, it is permissible to neglect the electron correction terms in the dispersion relation provided $\nu_e/|k_z v_e| < v_e/v_i$. If we put $k_z^{-1} = Rq$ we obtain $Rq/\lambda_{mfp} < v_e/v_i$ where $\lambda_{mfp} = v_e/\nu_e$ is the collisional mean free path. This condition is well satisfied in existing experiments.

## 5. EVALUATION OF TRANSPORT COEFFICIENTS

To estimate the transport coefficients derived in Section 4, we must make assumptions on the spectrum and amplitude of the mixing mode fluctuations. Our goal is to arrive at a set of coefficients that are simple enough to be used in a transport code, but still contain the major physical effects that are described by the linear and quasi-linear theories. First we shall estimate the fluctuation spectrum averages introduced in Section 4. This will yield a set of transport equations in which all the transport coefficients are expressed in terms of the common coefficient D given by Eq. (4-6). Then we shall give an evaluation of D by a rough estimate for the level of fluctuations.

To estimate the average quantities introduced in Section 4, we assume that the spectrum of fluctuations is peaked near the linearly most unstable wave vector, $\vec{k}_0$. Thus, $\ll A(\vec{k}) \gg \cong A(\vec{k}_0)$. Here we define the most unstable wavelength to be that of the mode which becomes unstable first as $\eta_i$ is increased. Errors will be introduced by this assumption because, in general, the spectrum of fluctuations will not be such that $\ll A(\vec{k}) \gg = A(\vec{k}_0)$. The error will be greatest if $A(\vec{k})$ varies appreciably over the extent of the spectrum in $\vec{k}$-space. In a later section, we shall discuss under what circumstances this situation may occur and what its effect on the overall rate of particle transport will be.

The specific values of $\vec{k}_0$ are obtained from the stability curves shown in Figs 2 and 4. We note that in both the collisional case of Fig.2 and the collisionless case of Fig.4 the modes with the smallest value of $k_z$ are most likely to be unstable. In addition, since we intend to simulate the modes that can be excited in a toroidal configuration and that are least affected by magnetic shear we take

$$k_{zo} \simeq (Rq)^{-1}$$

To assess $k_{y0}$ in the collisional case we consider Fig.2. For a given value of $(k_z r_n)^2 \nu_{**}$ the most unstable mode occurs for $\nu_{**} k_y^2 T_i/(m_i \Omega_i^2) \cong 0.25$. Thus, we take $\nu_{**} k_{y0}^2 T_i/(m_i \Omega_i^2) \cong 0.25$. To estimate $k_{y0}$ in the collisionless case we consider Fig.4. For a given value of $k_z r_n$ the most unstable mode occurs for $k_y^2 T_i/(\Omega_i^2 m_i) \cong 1.0$. Thus, we evaluate $k_{y0}^2 T_i/(m_i \Omega_i^2) \cong 1.0$. Given the estimates of $\vec{k}_0$ we now consider the expressions for the particle and energy fluxes derived in Section 4.

In Eq. (4-20) we take the coefficient of the convective term to be about unity. The coefficient of the conductive term can be assessed by examining the $k_y \rho_i$ dependence of K(b) as shown in Fig.6. In particular, for $b \to 0$ $K(b) \to 1.0$ and for $k_y \rho \approx \sqrt{2}$ $(b \cong 1)$ $K(1) = 0.10$. Thus, finite-Larmor-radius effects suppress the ion heat flux. Accordingly, we estimate $\ll Z(\zeta) K(b) \gg \cong 0.1 \pi^{1/2}$. For this evaluation of the anomalous ion thermal conductivity the assumption $\ll A(k) \gg = A(k_0)$ is somewhat strained. Clearly, if the unstable spectrum extends to values of $k_y$ lower than $k_{y0}$ the value of $\ll Z(\zeta) K(b) \gg$ will be greater than the $0.1 \pi^{1/2}$ estimated here. Accordingly, in Section 7, we examine the effect of underestimating the ion thermal conductivity by arbitrarily doubling our evaluation of $\ll Z(\zeta) K(b) \gg$. We may now write the particle and energy fluxes, valid in the collisionless regimes, as

$$\Gamma = - D \left( \frac{\partial n}{\partial x} - \frac{n}{2T_e} \frac{\partial T_e}{\partial x} \right) \tag{5-1}$$

$$Q_e = -nD \left( \frac{\partial T_e}{\partial x} + 2 \frac{T_e}{n} \frac{\partial n}{\partial x} \right) \tag{5-2}$$

$$Q_i = 2T_i \Gamma - 0.2 \left( \frac{v_e}{v_i} \right) \quad Dn \frac{\partial T_i}{\partial x} \tag{5-3}$$

Considering the collisional case of Eq. (4-25), we notice that the convective term appearing in it is dominated by the second term and we shall neglect it. We estimate $\ll \hat{\gamma} \gg = \nu_{**} k_{y0}^2 T_i/m_i \Omega_i^2$ from Fig. 2 to be 0.25. Thus, we obtain in the collisional limit:

$$\Gamma = -0.61 (Rq \nu_e / v_e) D \left( \frac{\partial n}{\partial x} - \frac{3}{2} \frac{n}{T} \frac{\partial T}{\partial x} \right) \tag{5-4}$$

$$Q_e = 0.62 \Gamma T_e \tag{5-5}$$

$$Q_i = - 0.28 \left( \frac{v_e}{v_i} \right) \quad D T_i \frac{\partial n}{\partial x} \tag{5-6}$$

To obtain expressions for the particle and energy fluxes that are approximately valid for arbitrary collisionality we combine the expressions valid in the collisional and collisionless regimes in the following way:

$$\Gamma = -D \{ (1+\nu_e^{**})^{-1} \left[ \frac{\partial n}{\partial x} - \frac{n}{2T_e} \frac{\partial T_e}{\partial x} \right] + 0.61 \nu_e^{**} \left[ \frac{\partial n}{\partial x} - \frac{3n}{2T_e} \frac{\partial T_e}{\partial x} \right] \} \tag{5-7}$$

$$Q_e = -nD\{(1+\nu_e^{**})^{-1}[\frac{\partial T_e}{\partial x} + \frac{1}{2}\frac{T_e}{n}\frac{\partial n}{\partial x}]$$

$$+ 0.38\nu_e^{**}[\frac{T_e}{n}\frac{\partial n}{\partial x} - \frac{3}{2}\frac{\partial T_e}{\partial x}]\} \qquad (5\text{-}8)$$

$$Q_i = 2T_i\Gamma - 0.2(1+\nu_e^{**})^{-1}(\frac{v_e}{v_i}) \quad Dn\frac{\partial T_i}{\partial x}$$

$$- 0.28\nu_e^{**}(1+\nu_e^{**})^{-1}(\frac{v_e}{v_i}) \quad DT_i\frac{\partial n}{\partial x} \qquad (5\text{-}9)$$

where $\nu_e^{**} = \nu_e Rq/v_e$. The collisional and collisionless fluxes correspond to the limits $\nu_e^{**} \gg 1$ and $\nu_e^{**} \ll 1$, respectively.

A precise calculation of D requires a complete theory of the fluctuations that result from the ion mixing mode instability but we shall limit ourselves to give only a crude estimate for D. In particular, we have calculated instability criteria that are of the form $\eta_i > \eta_c$, where $\eta_c$ is a function of local plasma parameters. Thus, we would like the mixing mode transport to be 'off' if $\eta_i < \eta_c$ and 'on' if $\eta_i > \eta_c$, with some smooth transition connecting the two states. To achieve this effect we write D as the product of a threshold function h and a diffusion coefficient $D_0$:

$$D = hD_o \qquad (5\text{-}10)$$

A possible model of the threshold function is

$$h = (\eta_i/\eta_c)^4/[1 + (\eta_i/\eta_c)^4] \qquad (5\text{-}11)$$

Thus, h increases from 0 to 1 as the plasma passes from a stable to an unstable state. This model of the transport resulting from a drift instability is similar to that proposed in Ref. [17].

The diffusion coefficient $D_0$ is obtained from Eq. (4-6) by specifying the maximum saturation level of mixing mode fluctuations. We assume that the mode growth will cease when the fluctuating $\vec{E} \times \vec{B}$ drift velocity becomes comparable to the equilibrium diamagnetic drift velocity. The level of fluctuation of the electrostatic potential under these circumstances is given by

$$|\frac{e\tilde{\phi}}{T_i}| \cong \Upsilon|k_y r_T|^{-1} \qquad (5\text{-}12)$$

where $T_i/r_T = dT_i/dr$. We introduce in the estimate a saturation parameter $\Upsilon$ that represents the uncertainty in the preceding argument. The effect of varying the quantity $\Upsilon$ is discussed in Section 7. Finally, putting $k_z \equiv (Rq)^{-1}$, Eq. (4-6) yields

$$D_o = \pi^{1/2}\Upsilon^2 D_B(\frac{T_i}{T_e})\frac{cT_i Rq}{eBv_e r_T^2}$$

where $D_B = cT_e/(eB)$.

Finally, we derive simplified expressions for the stability threshold $\eta_c$ that appears in Eq. (5-11). In the collisionless limit, we use a simplified form of Eq. (3-17)

$$\eta_{ia} = 1 + 5|r_n|/(Rq) \qquad (5\text{-}13)$$

Equation (5-13) is taken to apply for inverted profiles ($\eta_i < 0$) as well as for normal profiles ($\eta_i > 0$). The discrepancy between Eqs. (3-17) and (5-13) that exists for inverted profiles does not affect the transport calculations because, in practice, only large negative values of $\eta_i$ are encountered, and thus, inverted profiles are always unstable.

In the collisional limit the stability threshold implied by Fig.2 can be approximated by

$$\eta_{ib} = \mathrm{MAX}(2/3,\ 3.72(\nu_e^{**})^{1/2}|r_n|/R)$$

Combining the collisional and collisionless criteria we take

$$\eta_c = \frac{\eta_{ia} + \nu_e^{**}\eta_{ib}}{(1+\nu_e^{**})}$$

The expressions for the particle and energy fluxes, Eqs (5-6) – (5-9) as well as the expression for D, Eq.(5-10), can now be inserted into a one-dimensional radial transport code that describes the time evolution for a magnetically confined plasma column.

## 6. ONE-DIMENSIONAL TRANSPORT CODE

We have attempted to simulate the observed time evolution of the main plasma parameters in the Alcator toroidal device during gas injection experiments. We have incorporated the particle and heat transport associated with the ion mixing mode into a one-dimensional radial transport model. This model also contains the collisional (neoclassical) transport, including the Ware pinch, semi-empirical anomalous particle transport and electron heat transport, neutral-particle transport, ionization of neutrals and charge exchange

between neutrals and plasma ions, bremsstrahlung emission, a phenomenological representation of hydrogen and light impurity radiation loss, Ohmic heating, and collisional energy exchange between electrons and ions.

The model equations describing the time evolution of the plasma density n, of the electron and ion temperature $T_e$ and $T_i$, and of the poloidal magnetic field $B_\theta$ are as follows:

$$\frac{\partial n}{\partial t} = -\frac{1}{r}\frac{\partial}{\partial r}\left[r\left(\Gamma_{neo} + \Gamma_{an} + \Gamma_{mix}\right)\right] + nn_n\langle\sigma v\rangle_I \tag{6-1}$$

$$\frac{3}{2}\frac{\partial}{\partial t}(nT_e) = -\frac{1}{r}\frac{\partial}{\partial r}\left[r\left(Q^e_{neo} + Q^e_{an} + Q^e_{mix}\right)\right] + \frac{c}{4\pi r}E_z\frac{\partial(rB_\theta)}{\partial r} - 3\frac{m_e}{m_i}\frac{n}{\tau_e}(T_e - T_i) - e\Gamma_{neo}E_r - W^B_R - nn_n(\bar{W}_R + \bar{W}_I)\langle\sigma v\rangle_I \tag{6-2}$$

$$\frac{3}{2}\frac{\partial}{\partial t}(nT_i) = -\frac{1}{r}\frac{\partial}{\partial r}\left[r\left(Q^i_{neo} + Q^i_{an} + Q^i_{mix}\right)\right] + 3\frac{m_e}{m_i}\frac{n}{\tau_e}(T_e - T_i) + e\Gamma_{neo}E_r + \frac{3}{2}nn_nT_n\langle\sigma v\rangle_I - \frac{3}{2}nn_n(T_i - T_n)\langle\sigma v\rangle_{cx} \tag{6-3}$$

$$\frac{\partial B_\theta}{\partial t} = c\frac{\partial E_z}{\partial r} \tag{6-4}$$

$$E_r = \frac{T_i}{n}\frac{\partial n}{\partial r} - \frac{1}{e}(3/2 - y)\frac{\partial T_i}{\partial r} \tag{6-5}$$

Explicit expressions for some of the quantities appearing in the above equations are given in Ref. [15]. These include the ionization and charge-exchange reaction rates $\langle\sigma v\rangle_I$ and $\langle\sigma v\rangle_{cx}$, the bremsstrahlung radiation term $W^B_R$, the electron-ion collision time $\tau_e$, the neoclassical fluxes $\Gamma_{neo}$, $Q^e_{neo}$, and $Q^i_{neo}$, the parallel electric field $E_z$, and the parameter y. Here $n_n$ and $T_n$ are the density and temperature of neutrals. The effective ion charge $Z_{eff}$ is considered to be near 1.0 when simulating high-density Alcator discharges. The quantity $\bar{W}_I$ represents the plasma ionization potential (13.6 eV for hydrogen isotopes), and $\bar{W}_R$ similates the effects of line radiation, including contributions from light impurities. Its magnitude is based on ultraviolet and soft-X-ray measurements reported in Ref. [18], which indicate that the energy loss due to line radiation in Alcator discharges is approximately 10% of the total Ohmic power input. Thus,

$$\bar{W}_I\int_o^a nn_n\langle\sigma v\rangle_I r dr \approx 0.1\int_o^a j_z E_z r dr$$

where a is the limiter radius and $j_z = (c/4\pi r)\partial(rB_\theta)/\partial r$.

The anomalous fluxes $\Gamma_{an}$, $Q^e_{an}$ and $Q^i_{an}$ indicate the effects of modes other than the ion mixing mode and are chosen to have the following expressions:

$$\Gamma_{an} = -\alpha D_{an}\frac{\partial n}{\partial r} \tag{6-6}$$

$$Q^e_{an} = -nD_{an}\frac{\partial T_e}{\partial r} + \frac{5}{2}\Gamma_{an}T_e \tag{6-7}$$

$$Q^i_{an} = \frac{5}{2}\Gamma_{an}T_i \tag{6-8}$$

$$D_{an} = \frac{cT_e}{eB_z}\left[\frac{T_{eff}}{T_e}\frac{I(r)/\pi r^2}{nev_{the}} + \frac{c_1}{\nu^*_e}\right] \tag{6-9}$$

where $I(r) = crB_\theta/2$ is the current contained inside a radius r, $v_{the} = (2T_e/m_e)^{1/2}$, and $\nu^*_e = \sqrt{2}(R/r)^{3/2}Rq/(v_{the}\tau_e)$. In the expression for $D_{an}$, the first term within the brackets simulates the effects of current-driven drift modes and of collisional modes dominant in the outer region of the discharge. The second term roughly approximates the effects of trapped-electron modes. The magnitude of $D_{an}$ is not allowed to exceed the Bohm value $cT_e/eB_z$. A set of parameter values [5] which enables the model to simulate reasonably well the steady-state Alcator observations of energy confinement time and loop voltage reported in Refs [2, 18, 19] and the early time evolution of electron temperature during gas injection has been found by trial and error. It should be noted here that the discharge currents quoted in Ref. [18] are overestimated by about 15 percent [19]. Using the correct values, we have

$$\alpha \approx 0.2,\ T_{eff} \approx 15\ \text{eV},\ c_1 \approx 0.001$$

The particle and heat transport associated with the ion mixing mode are represented by the fluxes $\Gamma_{mix}$, $Q^e_{mix}$ and $Q^i_{mix}$, given by Eqs (5-7), (5-8), and (5-9). A value of the saturation parameter $\Upsilon^2$, see Eq. (5-12),

that effects a reasonable compromise between density rise rate during injection and steady-state electron and ion temperature is $\Upsilon^2 = 0.2$. We recall that the threshold function h depends on the local density, temperature, and their gradients.

The Monte-Carlo model for neutral-particle transport described in Ref. [20] is used in our calculation to determine the neutral density $n_n$ and neutral temperature $T_n$ as functions of radius for a given set of plasma parameters. In this model, test particles are launched in random directions from a point on the surface of an axisymmetric cylinder (simulating a tokamak). The volume of the cylinder is divided into a number of annular zones in which the plasma density and temperature are piecewise homogeneous. The test particles are tracked through the zones taking into account the effects of ionization (particle absorption) and charge exchange (change of velocity). Path length estimators are used to obtain the neutral density and temperature in each zone. The model has options for reflection of escaping neutrals and energy-dependent back-scattering of escaping ions as neutrals but these are not utilized here. We simply assume that there are two monoenergetic, isotropic sources of neutrals at the limiter. One source contributes a neutral influx equal to the outflux of plasma ions and charge-exchange neutrals at the limiter (perfect re-cycling and particle conservation). The other source is linearly related to the gas injection rate and provides the particles for the build-up of central density. Our calculations do not seem particularly sensitive to the energies of the neutral sources, and we have fixed both of them at 3 eV.

## 7. NUMERICAL SIMULATION

The radial transport model outlined previously has been incorporated into a computer code which obtains numerical solutions for the plasma parameters n, $T_e$, $T_i$ and $B_\theta$ for a prescribed set of initial conditions and boundary conditions. A discussion of the numerical procedures that we have utilized to solve the transport equations can be found in Ref. [15]. Some of the coding was taken directly from a modified version of the Düchs transport code [21].

In our code, the boundary conditions for the plasma parameters at r = 0 and r = a (the limiter radius) are prescribed as follows:

$$\frac{\partial n}{\partial r}(0) = 0 \qquad \frac{\partial n}{\partial r}(a) = 0$$

$$\frac{\partial T_e}{\partial r}(0) = 0 \qquad T_e(a) = \text{const.} = 10 \text{ eV}$$

$$\frac{\partial T_i}{\partial r}(0) = 0 \qquad T_i(a) = T_e(a)$$

$$B_\theta(0) = 0 \qquad B_\theta(a) = f(t)$$

where f(t) reflects the imposed time dependence of the total discharge current. The inward flux of cold neutrals representing gas injection can also be programmed to be an arbitrary function of time. We call attention to the use of the zero-gradient condition $\partial n(a)/\partial r = 0$ instead of the more usual pedestal condition n(a) = const. Test calculations show that the behaviour of the plasma parameters for $r < 0.8$ a is essentially unaffected by the choice of the density boundary condition even though the outflux of plasma ions and the influx of re-cycled neutrals are highly dependent on this choice. This result remains true when the energy of incoming neutrals is raised to 30 eV in our code, in contrast to suggestions elsewhere (e.g. Ref. [20]) that an influx of energetic re-cycled neutrals is crucial for the build-up of plasma density. However, the zero-gradient condition allows the value of n(a) to increase as the total number of plasma particles increases, in qualitative agreement with experimental observations made in the vicinity of the limiter on Alcator [19]. For numerical reasons we have found it advantageous to set the mixing mode diffusion coefficient $D_0$ equal to zero at r = a and at the last finite difference grid point before r = a. If this is not done, numerically unstable behaviour near the boundary can occur because of inward particle and heat fluxes.

At t = 0, the initial profiles for n, $T_e$ and $T_i$ are empirically chosen to match low-density Alcator observations. The initial profile for $B_\theta$ is defined by approximating the parallel current density $j_z(r)$ as

$$j_z(r) \approx \alpha(1-r^2/a^2)^3$$

and writing

$$B_\theta = B_\theta(a)\, a \int_0^r r j_z dr / (r \int_0^a r j_z dr)$$

As time evolves, however, the memory of the initial profiles is lost and their choice is not a critical one. Throughout our calculations, we have fixed the limiter radius a to be 9 cm.

In the Alcator experiments that we have simulated cold neutral deuterium gas is bled into the vacuum chamber at a constant rate for a specified time interval, resulting in observed increases of line-average and central plasma density. The neutral throughput is

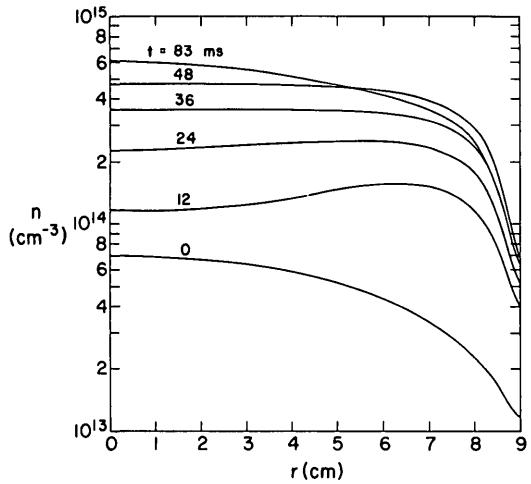


*FIG.7. Radial dependence of plasma density during and after neutral-gas injection ($\Upsilon^2 = 0.2$). The saturation parameter $\Upsilon$ is defined by Eq. (5–12).*

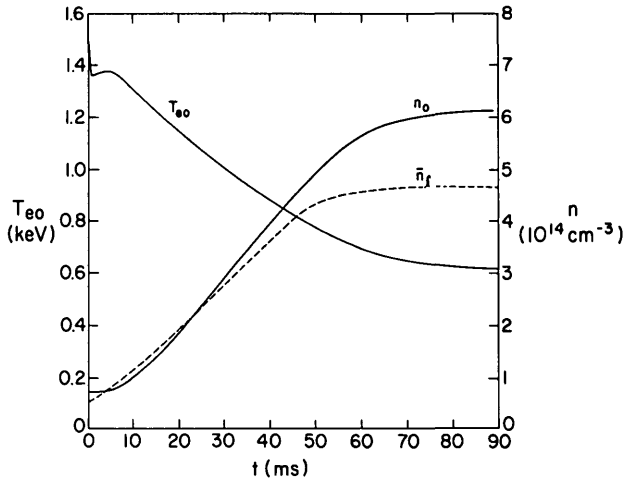


*FIG.10. Time dependence of central and line-average plasma density $n_0$ and $\bar{n}_\ell$ and central electron temperature $T_{e0}$ ($\Upsilon^2 = 0.2$).*

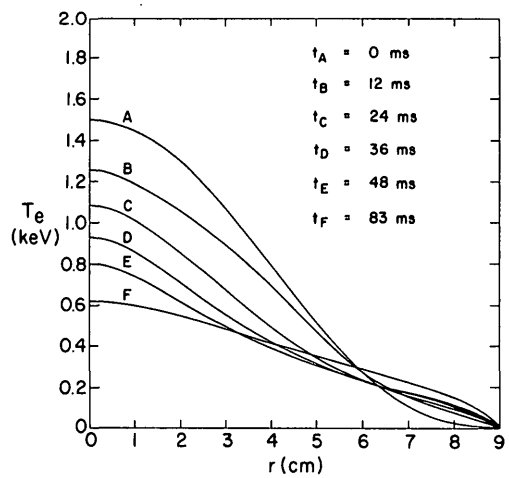


*FIG.8. Radial dependence of electron temperature during and after neutral-gas injection ($\Upsilon^2 = 0.2$).*

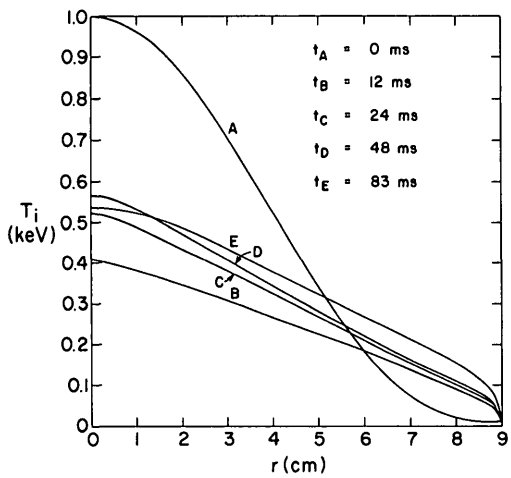


*FIG.9. Radial dependence of ion temperature during and after neutral-gas injection ($\Upsilon^2 = 0.2$).*

then reduced to a level sufficient to balance the loss of plasma particles. This produces a steady-state density profile after a relaxation period of ~ 20 ms. The plasma current is slowly increased during the period of density rise to avoid disruption of the discharge by macroscopic instabilities as described in the introduction. In our computational simulation, we have chosen the inflow rate of 3 eV neutral gas at the limiter to be $3 \times 10^{13}$ cm$^{-2}$·ms$^{-1}$ during plasma build-up, resulting in an area-average density rise rate of $6.67 \times 10^{12}$ cm$^{-3}$·ms$^{-1}$ for a = 9 cm and perfect re-cycling conditions. After 48 ms, the neutral inflow is reduced to zero, and steady state is achieved by perfect re-cycling. The total plasma current is increased linearly from 116 kA to 136 kA during build-up. The toroidal magnetic field is set at 60 kG.

In Figs 7 to 9, we show the time evolution of the radial profiles for plasma density, electron temperature, and ion temperature predicted by the code. The curves for t = 83 ms represent the 'steady-state' density and temperature profiles which develop after the neutral inflow is turned off at t = 48 ms. Figure 10 shows the time dependence of the central and line-average plasma densities $n_0$ and $\bar{n}_\ell$, and the central electron temperature $T_{e0}$.

These results may be compared with the experimental observations as reported in Refs [18, 19] and [22, 23]. The calculated steady-state density and temperature profiles are in reasonable agreement with the data, although the electron and ion temperatures near r = 7.6 cm are too high by about a factor of two.

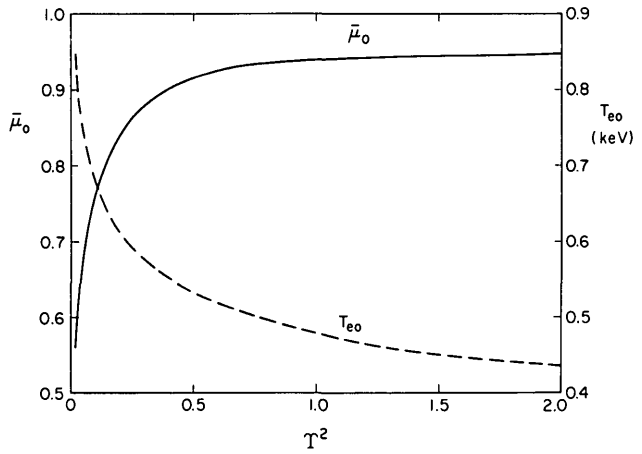


*FIG.11. Average rise rate $\bar{\mu}_0$ of central density during gas injection and steady-state central electron temperature $T_{e0}$ as functions of saturation parameter $\Upsilon^2$. $\bar{\mu}_0$ is measured in units of $10^{14}$ cm$^3$/10 ms. The saturation parameter is defined by Eq. (5–12).*

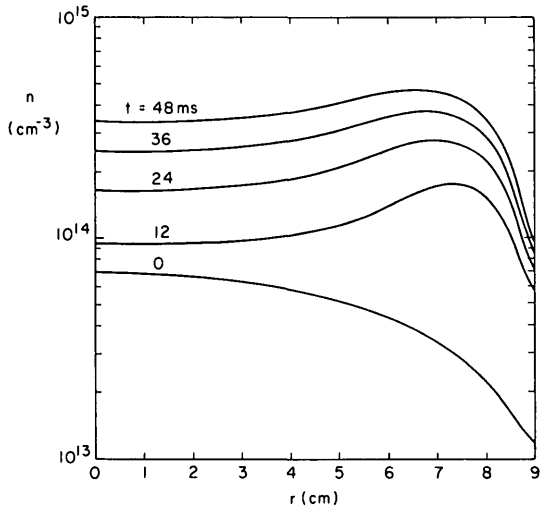


*FIG.12. Radial dependence of plasma density n during neutral-gas injection ($\Upsilon^2$ = 0.02).*

The loop voltage, energy confinement time, and line-average density for the steady-state profiles are found to be 2.8 V, 13 ms, and 4.6 X $10^{14}$ cm$^{-3}$ respectively. If a simulation is performed in which the neutral influx is turned off after 18 ms (but with the final discharge current still equal to 136 kA), these quantities are 1.9 V, 11 ms, and 2.1 X $10^{14}$ cm$^{-3}$. The calculated density profiles during gas injection are rather flat, with a slight inversion at early times (Fig.7). The rise rate of the central density during injection is not uniform in time and has an average value of 0.84 X $10^{14}$ cm$^{-3}$/10 ms. In the actual experiments, the density profiles appear to maintain an approximately parabolic shape during injection, in many cases steepening slightly at high values of the average density. For a rate of increase of area average density roughly equivalent to that assumed in our simulation, the observed rise rate of the central density in Alcator is about 1.33 X $10^{14}$ cm$^{-3}$/10 ms. Thus our simulation somewhat underestimates the rise of the central density, reflecting the relative flatness of the calculated profiles.

It is important to consider the quantitative effects of varying the saturation parameter $\Upsilon^2$ and the threshold function h in our model. These quantities are not specified by the theoretical treatment of the ion mixing mode given previously. Qualitatively, it is apparent that increasing (decreasing) $\Upsilon^2$ should result in increased (decreased) inward particle transport and outward heat transport. This behaviour is reflected in Fig.11 which shows the average rise rate of neutral density during injection $\bar{\mu}_0$ and the steady-state central electron temperature $T_{e0}$ as functions of $\Upsilon^2$. The fact that $\bar{\mu}_0$ does not increase appreciably for $\Upsilon^2 \gtrsim 0.7$ corresponds to the fact that the rate of inward particle transport due to the ion mixing mode becomes equal to or larger than the rate of admission of neutral atoms into the plasma chamber. On the other hand, the ion thermal conductivity continues to increase and, correspondingly, $T_{e0}$ continues to deteriorate. As $\Upsilon^2$ is decreased, the density profiles during injection become more strongly inverted in the outer region of the discharge. This is illustrated in Fig.12 where $\Upsilon^2$ = 0.02. Numerical experiments (e.g. changing the exponent from 4 to 8 in expression (5-11))imply that our simulation results are quite insensitive to the precise form of the threshold function h, provided h retains a step function character.

Since several details of the ion mixing mode model are admittedly the result of some rather crude theoretical procedures, it is important to determine the effects of variations in these details on our calculations. In one group of numerical experiments, the effect of altering the various stability criteria was investigated. We first replaced the factor 5 in expression (5-12) for the collisionless stability threshold with 0 and then with 20 ($\Upsilon^2$ = 0.2). The results of the first experiment show very little change from the 'standard' case. In the second experiment, the average rise rate of central density $\bar{\mu}_0$ decreased by 13% and the central steady-state electron temperature $T_{e0}$ increased by 30%. In another experiment, we changed the factor 2/3 in the expression (5-13) for the collisional stability criterion to 3. Here, $\bar{\mu}_0$ decreased by 9% and $T_{e0}$ increased by 5% from the standard case. Finally, the effect of an

underestimate of the mixing mode ion thermal conductivity was determined. We recall that in Section 5 we estimated the quantity K(b) to be 0.1. However, this assessment relied on the spectrum of fluctuations being sharply peaked at $k_\perp \sim \rho_i$, and it was determined that a broader spectrum extending to longer perpendicular wavelengths would produce a larger thermal conductivity. Accordingly, we doubled our estimate of K(b). That is, we changed the factor 0.2 that appears in Eq. (6-12) for the mixing mode ion heat transport to 0.4. The main result was a decrease of about 5% in both $T_{e0}$ and $T_{i0}$ (the steady-state central ion temperature).

## 8. CONCLUSION AND DISCUSSION

We now comment on the possible connection between recently observed edge density fluctuations in the Alcator [24] and ATC [25] experiments and the ion mixing mode. The frequencies and wavelengths of the observed fluctuations are indicative of drift wave disturbances. However, a possible identification of the excited modes is made difficult by the presence of effects such as those of strong inhomogeneities, ambipolar electric fields, non-linearities, etc. An identification of the ion mixing mode is further complicated by the facts that the wave is highly dispersive for all wavelengths and that its growth rate in the linear regime is comparable to the oscillation frequency. A possible signature for this mode is that its phase velocity is in the direction of the ion diamagnetic velocity and its frequency $\omega$ should be about $|k_\parallel v_i|$, with $k_\parallel \gtrsim 1/qR_0$ and its transverse wave number $k_\perp \lesssim \rho_i^{-1}$.

Recalling the expression for the coefficient D given by Eq. (5-10) and its relation to the fluctuation level given by Eq. (4-6), we can calculate the radial profile of the fluctuation level implied by our model, as

$$\left|\frac{\tilde{n}}{n_o}\right|^2 = h(r)' \{\Upsilon T_i/[k_{yo} r_{T_i} T_e]\}^2$$

A representation of the fluctuation level profile for two different times during the 'standard' ($\Upsilon^2 = 0.2$) Alcator simulation discussed previously is shown in Fig.13. Clearly, the fluctuations are concentrated near the edge of the device, which is consistent with the observations of Ref. [24]. Also, the amplitude of the fluctuations required to produce the observed inward transport is consistent with that measured directly. Thus, we find the agreement between our theory and experimental observations of density fluctuations to be encouraging.

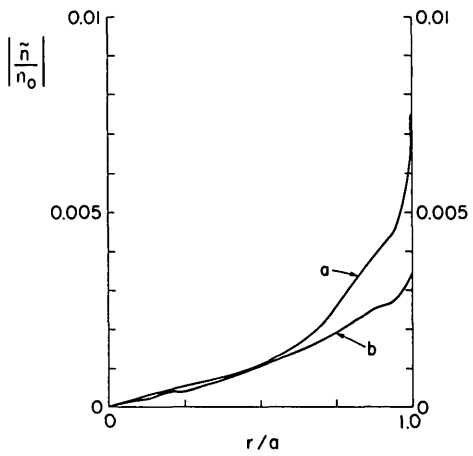


*FIG.13. Radial dependence of ion mixing mode fluctuation level during and after neutral-gas injection ($\Upsilon^2 = 0.2$) for a) t = 25 ms and b) t = 89 ms. Here we have taken $T_e = T_i$ in Eq. (8–1), for simplicity.*

As a final point, we argue that the assumed cold-plasma layer can act as an effective shield against the transport of impurities toward the centre of the plasma column. The observable impurity distribution should result from a balance of the effect of collisions that tend to carry impurities inward and the effects of collective modes that produce an outward impurity flux. A complete discussion of the impurity-driven modes that can be excited in the regimes of interest has been given in Ref. [8], and we shall not attempt to repeat it here. We recall only that the minimum values of $\eta_i$ for which the relevant anomalous transport is outward is 2/3 and that the general nature of impurity-driven modes bears a strong resemblance to that of the ion-temperature-gradient-driven modes that we have treated in this paper.

## ACKNOWLEDGEMENTS

It is a pleasure to thank T. Schep and C. Spight for their collaboration during the early phase of this work. This work was sponsored in part by the US Department of Energy.

## REFERENCES

[1] COPPI, B., Comments Plasma Phys. Contr. Nucl. Fusion 3 (1977) 47; COPPI, B., Phys. Fluids 8 (1965) 2273.
[2] HOSEA, J., private communication (1974).
[3] BOXMAN, G., COPPI, B., DEKOCK, L., MEDDENS, B., OOMENS, A., ORNSTEIN, L., PAPPAS, D., PARKER, R.,

PIERONI, L., SEGRE, S., SCHULLER, F., TAYLOR, R., in Controlled Fusion and Plasma Physics (Proc. 7th Europ. Conf. Lausanne, 1975).
[4] COPPI, B., SPIGHT, C., Phys. Rev. Lett. **41** (1978) 551.
[5] COPPI, B., TARONI, A., Heating of Thermonuclear Plasmas (Proc. 1976 Varenna Conf.) in Publ. Editrice Compositori, Bologna, Italy (1977).
[6] RUDAKOV, I., SAGDEEV, R.Z., Dokl. Akad. Nauk SSSR **138** (1961) 581 [Sov. Phys.-Dokl. **7** (1961) 417].
[7] COPPI, B., ROSENBLUTH, M.N., SAGDEEV, R.Z., Phys. Fluids **10** (1967) 582.
[8] COPPI, B., REWOLDT, G., SCHEP, T., Phys. Fluids **19** (1976) 1144.
[9] HORTON, C.W., Jr., VARMA, R.K., Phys. Fluids **15** (1972) 620.
[10] BRAGINSKII, S.I., in Reviews of Plasma Physics (LEONTOVICH, M.A., Ed.) Vol. 1, Consultants Bureau, New York (1966) 205.
[11] FRIED, B., CONTE, S., The Plasma Dispersion Function, Academic Press, New York (1961).
[12] KRALL, N.A., ROSENBLUTH, M.N., Phys. Fluid **8** (1965) 1488.
[13] COPPI, B., ROSENBLUTH, M.N., SAGDEEV, R.Z., Phys. Fluids **10** (1967) 582; RUTHERFORD, P.H., FRIEMAN, E.A., Phys. Fluids **14** (1971) 134.
[14] COPPI, B., Phys. Rev. Lett. **39** (1977) 939.
[15] ANTONSEN, T., COPPI, B., ENGLADE, R., Inward Particle Transport by Plasma Collective Modes, Massachusetts Institute of Technology Report PRR-78/29, July 1978.
[16] MANHEIMER, W.M., An Introduction to Trapped-Particle Instability in Tokamaks, ERDA Critical Review Series T1D-27157, National Technical Information Service, Washington, DC (1977).
[17] MANHEIMER, W.M., ANTONSEN, T.M., Jr., Electron Energy Confinement in Tokamaks, NRL Memo Report 3551 Naval Research Laboratory, Washington, DC (1978).
[18] GAUDREAU, M., GONDHALEKAR, A., HUGHES, M.H., OVERSKEI, D., PAPPAS, D.S., PARKER, R.R., WOLFE, S.M., APGAR, E., HELAVA, H.I., HUTCHINSON, I.H., MARMAR, E.S., MOLVIG, K., Phys. Rev. Lett. **39** (1977) 1266.
[19] OVERSKEI, D., private communication (1978).
[20] HUGHES, M.H., POST, D.E., A Monte Carlo Algorithm for Calculating Neutral Gas Transport in Plasmas, Princeton Plasma Physics Laboratory Report PPPL-1335, Princeton, N.J. (1977).
[21] DÜCHS, D.F., POST, D.E., RUTHERFORD, P.H., Nucl. Fusion **17** (1977) 565.
[22] GONDHALEKAR, A., private communication (1978).
[23] HUGHES, M.H., Numerical Calculations of Transport in Alcator, Princeton Plasma Physics Laboratory Report PPPL-1411, Princeton, N.J. (1972).
[24] SLUSHER, R.E., SURKO, C.M., Phys. Rev. Lett. **40** (1978) 400.
[25] SURKO, C.M., SLUSHER, R.E., Phys. Rev. Lett. **37** (1977) 1747.

(Manuscript received 28 August 1978
Final version received 15 January 1979)